


ORIGINAL RESEARCH

Optical gas imaging and deep learning for quantifying enteric methane emissions from rumen fermentation in vitro

Mohamed G. Embaby¹ | Toqi Tahamid Sarker²  | Amer AbuGhazaleh¹ |
Khaled R. Ahmed²

¹School of Agricultural Sciences, Southern Illinois University Carbondale, Illinois, USA

²School of Computing, Southern Illinois University Carbondale, Illinois, USA

Correspondence

Toqi Tahamid Sarker, School of Computing, Southern Illinois University Carbondale, IL, USA.
Email: toqitahamid.sarker@siu.edu

Funding information

National Institute of Food and Agriculture, Grant/Award Number: 2022-70001-37404; Office of the Vice Chancellor for Research at Southern Illinois University Carbondale

Abstract

This study investigated the possibility of using a laser methane detector (LMD) and optical gas imaging (OGI) to detect and quantify enteric methane (CH_4) produced by ruminants in vitro. Four single-flow continuous fermenters were used for rumen culture incubation with four different treatment diets: Control (50:50 forage to concentrate [F:C] ratio), Control + Bromoform (CBR), Low Forage (LF; 20:80), and High Forage (HF; 80:20). After 10 days of incubation, all fermenter contents were transferred and used in a 24 h ANKOM batch culture to measure CH_4 gas production with LMD and OGI. The authors introduce the Controlled Diet (CD) dataset, a large-scale collection of 4,885 CH_4 plume images captured using an FLIR GF77 OGI camera under varying dietary conditions. The performance of six semantic segmentation models (FCN, U-Net, Vision Transformer, Swin Transformer, DeepLabv3+, and Gasformer) on the CD dataset is compared. Results showed that LMD data for CH_4 followed a similar pattern to the gas chromatography (GC) instrument results. The in vitro results showed that different diets and F:C ratios had an impact on CH_4 gas production and rumen fermentation characteristics. Adding bromoform to the control diet fully inhibited CH_4 emission. The HF diet produced more CH_4 compared to all treatments ($p < 0.01$) when measured with GC and LMD. CBR produced the lowest CH_4 values when measured with GC and LMD. The Gasformer architecture achieved the highest performance with mean IoU of 85.1% and mean F-score of 91.72%. These findings demonstrate that OGI technology combined with advanced semantic segmentation models offers a promising solution for predicting and quantifying CH_4 emissions in the livestock sector, potentially aiding in the development of mitigation strategies to combat climate change.

1 | INTRODUCTION

Methane (CH_4) emissions produced by ruminant animals are contributing significantly to global climate change. The ability of CH_4 to warm the atmosphere is 36 times greater than carbon dioxide (CO_2) [1]. Ruminant contribution to global climate change is estimated to be about 6% of global climate emissions [2]. CH_4 is a byproduct of enteric fermentation that takes place in the rumen. It is also estimated that the produced CH_4 accounts for about 6–12% of lost energy that could be redirected for the production of milk and meat [3]. Researchers and governments have been working jointly to reduce the

impact of CH_4 on the environment. Several mitigation strategies have been developed by scientists to decrease enteric CH_4 production from ruminant animals [2]. Some of these strategies focus on manipulating animal feed, while others focus on targeting the methanogens that produce CH_4 during the fermentation process. Evaluating the efficacy of these mitigation strategies requires using precise methods and techniques for CH_4 detection and quantification.

Conventional methods for measuring CH_4 emissions from livestock include the use of CH_4 gas chambers, ventilated hoods, gas chromatography (GC) machines, and laser methane detectors (LMD) [4–6]. While these methods have been widely employed, they often pose challenges due to their complexity, high costs, and limited scalability.

Mohamed G. Embaby and Toqi Tahamid Sarker contributed equally to this work.

This is an open access article under the terms of the [Creative Commons Attribution-NonCommercial-NoDerivs](https://creativecommons.org/licenses/by-nc-nd/4.0/) License, which permits use and distribution in any medium, provided the original work is properly cited, the use is non-commercial and no modifications or adaptations are made.

© 2025 The Author(s). *IET Image Processing* published by John Wiley & Sons Ltd on behalf of The Institution of Engineering and Technology.

To address these limitations, researchers have explored advanced imaging technologies that enable non-invasive and scalable CH₄ detection. Recent advancements in multi-spectral and hyperspectral imaging across the visible to short-wave infrared spectrum (SWIR) have emerged as powerful tools for CH₄ detection and quantification. While multi-spectral cameras provide broad spectral coverage with limited bands, making them primarily suitable for detecting higher concentration CH₄ plumes (typically above 200–300 kg/h), hyperspectral imaging in the SWIR region (2.2–2.4 μm) enables detection of subtle CH₄ absorption features at much lower concentrations that are invisible to traditional imaging methods. Kumar et al. [7] proposed Hyperspectral Mask-RCNN, which processes hyperspectral data through multiple matched filters and ensemble learning to detect CH₄ plumes, achieving 87% intersection-over-union (IoU) with expert annotations while reducing manual processing time by 12x. Building upon this work, Kumar et al. [8] introduced MethaneMapper, a spectral absorption-aware transformer architecture that effectively combines both spectral and spatial correlations to accurately delineate CH₄ plumes. Their approach achieved 63% mean Average Precision (mAP) while reducing model size by 5x compared to previous methods. In the satellite domain, Rouet-Leduc and Hulbert [9] demonstrated that vision transformers applied to multi-spectral Sentinel-2 data could detect CH₄ plumes down to 200–300 kg/h, achieving an order of magnitude improvement over traditional band-ratio methods. Their approach enables automated CH₄ monitoring at a global scale with high temporal resolution (2–5 days revisit time) and fine spatial resolution (20 meter pixel size), providing a significant advancement towards systematic quantification of atmospheric CH₄. However, the limited spectral resolution of multi-spectral sensors remains a constraint for detecting very low concentration CH₄ emissions typical in livestock applications.

Building upon these imaging advances, artificial intelligence techniques have emerged as powerful tools for analyzing complex CH₄ data. Computer vision, deep learning, and machine learning techniques have found applications in various aspects of agriculture [10–12] and farm management [13–16], including monitoring animal productivity, reproduction, and health in the livestock sector [17, 18].

In the specific context of CH₄ detection, Jongaramrungruang et al. [19] developed MethaNet, a convolutional neural network (CNN) model that directly quantifies CH₄ point-source emissions from high-resolution 2-D plume imagery without relying on wind speed measurements. In the context of livestock, Ramirez-Agudelo et al. [20] investigated the potential use of intake time as a predictor of enteric CH₄ emissions in cattle using a CNN based on the YOLO [21] architecture. Jeong et al. [22] use a U-Net [23] architecture for image segmentation to estimate dairy CH₄ emissions from California's San Joaquin Valley using aerial imagery.

While these AI approaches have shown promise with various imaging modalities, OGI cameras have emerged as another powerful tool for CH₄ detection and quantification, enabling the visualization of CH₄ plumes that are invisible to the naked eye. Wang et al. [24] developed GasNet, a CNN-based approach

for automatic CH₄ leak detection from OGI videos, achieving high detection accuracy across various leak sizes and imaging distances. In a subsequent study, Wang et al. [25] extended the capabilities of infrared camera technology by developing VideoGasNet, a 3D CNN that automatically classifies the size of CH₄ leaks with high accuracy. However, these studies primarily focused on capturing CH₄ gas with OGI cameras at relatively high flow rates, which are more commonly associated with industrial leaks. In contrast, detecting and quantifying CH₄ emissions from livestock, which typically have much lower flow rates, presents a unique challenge that requires further investigation and the development of specialized techniques. In our previous work, Sarker et al. [16] addressed this research gap by proposing Gasformer, a transformer-based semantic segmentation architecture that uses OGI to detect and quantify CH₄ emission from a CH₄ calibration gas cylinder and detect CH₄ from dairy cow rumen gas samples. While Gasformer demonstrated effectiveness in quantifying low-flow CH₄ emissions from a controlled gas cylinder, it could only detect CH₄ emissions from a limited dataset of 340 images captured from dairy cow rumen gas without the ability to quantify the emissions. Further research is needed to push the boundaries of CH₄ emission detection and quantification in the livestock sector, particularly at very low concentrations across different diets, using a larger dataset.

To the best of our knowledge, no research has combined OGI and deep learning techniques to detect and quantify CH₄ emissions from livestock at very low concentrations under different dietary conditions using a large-scale dataset. This article aims to address this gap by using computer vision and deep learning to detect and quantify CH₄ gas emitted from dairy cattle in vitro, where quantification is achieved through the classification of emissions into GC-validated concentration ranges, focusing on very low concentrations of CH₄ gas. This approach enables accurate categorization of CH₄ emissions based on established concentration ranges, with GC validation ensuring precise measurement standards.

We investigate the possibility of using an LMD and OGI to detect and quantify enteric CH₄ produced by ruminants in vitro. We use four single-flow continuous fermenters for rumen culture incubation, with four different treatment diets added to each fermenter. We capture CH₄ plume images using a FLIR GF77 OGI camera and develop a novel large-scale dataset called the Controlled Diet (CD) dataset. This dataset consists of 4885 images of CH₄ gas collected from the continuous culture fermenter system under varying dietary conditions. In comparison to the work of Sarker et al. [16], our dataset represents a significant advancement by not only providing a substantially larger number of images but also incorporates the impact of different diets on CH₄ emissions, enabling a more comprehensive analysis of the factors influencing CH₄ production in livestock.

It is important to note that while our deep learning approach provides a method for quantifying CH₄ plumes through concentration range analysis, the actual measurement of CH₄ concentrations is performed using Gas Chromatography (GC) and laser detection (LMD). The semantic segmentation model serves as a supporting tool for visualizing and

categorizing emissions based on these measured concentration ranges, rather than directly measuring CH₄ concentrations from the images.

To detect and quantify the CH₄ plumes, we utilize six state-of-the-art semantic segmentation models: Fully Convolutional Network (FCN) [26], U-Net [23], DeepLabv3+ [27], Vision Transformer [28], Swin Transformer [29] and Gasformer [16]. We compare the performance of these models using evaluation metrics such as mean Intersection over Union (mIoU) and mean F-score (mFscore) and analyze their computational efficiency by considering frames per second (FPS) on GPU, giga floating point operations (GFLOPs) and the number of parameters.

The main contributions of this article are as follows:

1. We present a novel approach for detecting and quantifying enteric CH₄ emissions from ruminants in vitro using LMD and OGI, validated by GC analysis.
2. We introduce the CD dataset, which consists of CH₄ plume images captured using a FLIR GF77 OGI camera, categorized by GC-measured concentration ranges.
3. We compare the performance of six semantic segmentation models on the CD dataset, demonstrating the effectiveness of the Gasformer architecture in accurately segmenting CH₄ plumes across different GC data range classes.

The remainder of this article is organized as follows. Section 2 describes the materials and methods used in this study, including the continuous culture system preparation and batch culture system preparation. Section 3 describes the LMD data logs, dataset collection, mask generation, and statistical analysis. Section 4 discusses Gasformer architecture and model training. Section 5 presents the results of the in vitro batch experiments, LMD readings, and the performance of the semantic segmentation models on the CD dataset. Section 6 discusses the findings, limitations, and future research directions. Finally, Section 7 concludes the article.

2 | MATERIALS AND METHODS

2.1 | Continuous culture system preparation

Four different treatments were incubated in four single-flow continuous fermenters as described by Teather and Sauer [30]. Treatments were: control with a 50:50 forage to concentrate (F:C), control + bromoform (CBR) (0.14 μ L/liter of rumen fluid/day) added to 50:50 F:C ratio, low forage (LF) diet consisting of 20% forage diet and 80% concentrate, and high forage (HF) diet consisting of 80% forage and 20% concentrate mix. The incubation period lasted for 10 days. Continuous fermenters were used as a simulation for cow rumen. Every fermenter consisted of 700 mL of rumen liquor collected from a fistulated dairy cattle that receive a total mixed ration that consists of 50:50 F:C mix diet. The forage diet consisted of alfalfa pellets, while the concentrate mix ingredients are listed in Table 1. Each fermenter received 54 gm of diet three times daily at 0800, 1500, and 2400 h to maintain bacterial growth and

TABLE 1 Concentrate mix ingredients.

Ingredient	g/kg (dry matter basis)
Ground corn	560
Soybean meal, 48% CP	260
Soybean hulls	160
Mineral mix ^a	10
Limestone	10

^aMineral mix Purina (wind & rain). All season 7.5 complete. © 2024 Purina Animal Nutrition LLC.

good fermentation. A CO₂ gas tank was connected to provide a continuous flushing of CO₂ to maintain aerobic conditions necessary for bacterial survival. To avoid acid accumulation inside the fermenter as a result of microbial fermentation of food, all fermenters received artificial saliva as described by McDougall [31]. The saliva buffer was pumped at a rate of 70 mL/h using a peristaltic pump (BT100F-1, manufactured by GOLANDER, 4405 International Blvd. Ste B117 Norcross, GA 30093, USA). The fermenter temperature was kept at 39°C using a circulating water batch, while the feed motility inside the fermenter was maintained using an automatic stirrer (Fisher, St. Louis, MO, USA) set at 45 RPM to guarantee the accessibility of rumen microbes to nutrients. pH was recorded daily at feeding time using a portable pH meter (OAKTON Instruments, Vernon Hills, IL, USA). After 10 days of incubation, all fermenter contents were used in a 24-h batch culture experiment to measure gas production and rumen fermentation characteristics.

2.2 | Batch culture system preparation

Total gas production was measured through a 24-h ANKOM batch culture using the fermenters' content as rumen culture, and gas samples for the evaluation of CH₄ production were also collected. The batch culture system is designed by ANKOM incubation (ANKOM Technology, Macedon, NY). 100 mL of rumen liquor was incubated with 100 mL of buffer [31], and 3 gm of the same treatment diet fed to the fermenters. All ANKOM modules were flushed with CO₂ to maintain anaerobic conditions, then moved to a 39°C water bath to keep the bacteria at optimal temperature. Following the incubation, TEDLAR gas bags (CEL Scientific Corp., Santa Fe Springs, CA, USA) were connected to each module to collect the emitted gas required for CH₄ analysis. After 24 h of incubation, all gas bags are collected and analyzed using the gas chromatography instrument developed by SRI instrument (SRI 8610C, Torrance, CA, USA). 1 mL of gas is drawn from each bag and injected into the GC analysis port. The GC machine is equipped with a thermal conductivity detector (6' x1/8' S.S. Shin Carbon), and a two-meter Hay-D column was installed with a 1/8 in. OD, 2 mm ID, 6 feet Haysep D packing, mesh size 80/100, pre-conditioned. The GC was programmed to run for 3 min at 50°C, while argon was used as a carrier gas, and 3 gas peaks were identified (Hydrogen (H₂), CH₄, and CO₂). Gases are reported as a percentage

of total gas. Total gas production was calculated using the automated system of the ANKOM gas production system, and the following formula was applied to convert the PSI values to mL of gas:

$$n = p \left(\frac{V}{RT} \right), \quad (1)$$

where n is the gas produced in moles (mol), p is the pressure in kilopascals (kPa), V is the headspace volume in the glass bottle in liters (L), T is the temperature in Kelvin (K), and R is the gas constant ($8.314472 \text{ L kPa K}^{-1} \text{ mol}^{-1}$).

The dry matter digestibility was measured by collecting and weighing the outflow at the last 3 days. Samples for volatile fatty acids (VFA) and ammonia nitrogen ($\text{NH}_3\text{-N}$) were collected after 24 h of incubation. 4 mL of sample were mixed with 1 mL of 25% meta-phosphoric acid as described by Jenkins [32]. All samples were kept in freezers. At the end of the experiment, all samples were thawed, and 2 mL of each sample was centrifuged at $13,000g$ for 15 min. Following the centrifuge step, 1 mL of the sample was moved to GC vials, while 0.1 mL of 2-ethylbutyric acid was added as an internal standard. All VFA samples were run through a GC machine manufactured by Shimadzu GC-2010 gas chromatograph (Shimadzu Scientific Instruments Inc., Columbia, MD, USA), with a 30-m SP-2560 fused silica capillary column (Restek Stabil WAXDA column, Bellefonte, PA, USA). The GC temperature was programmed to 65°C for 3 min, increased at $12^\circ\text{C}/\text{min}$ to a final temperature of 180°C with an overall 12-min running time for each sample. The column temperature was maintained at 65°C , and the flame ionization detector temperature was at 225°C .

3 | DATASET

Following the CH_4 gas generation from our experimental setup, we established a comprehensive data collection and analysis pipeline. This section details our approach to data collection using both laser methane detection and optical gas imaging, along with the statistical analyses and mask generation procedures used to prepare the dataset for deep learning applications.

3.1 | Laser data logs

For quantifying CH_4 gas produced in the ANKOM incubation modules, we used the GAS · TRAC® LZ-30 laser methane detector. The detector utilizes Tunable Diode Laser Absorption Spectroscopy technology with the following key operational parameters: detection sensitivity of $5 \text{ ppm} \cdot \text{m}$ at distances up to 15 m and $10 \text{ ppm} \cdot \text{m}$ at distances up to 50 m for concentrations above $300 \text{ ppm} \cdot \text{m}$, with a measurement range of $0\text{--}50,000 \text{ ppm} \cdot \text{m}$ in $1 \text{ ppm} \cdot \text{m}$ increments. The response time is less than 0.1 s, enabling real-time monitoring. The device operates optimally within a temperature range of -20°C to 45°C and features a conical beam with a 20 cm diameter at 30 m distance.

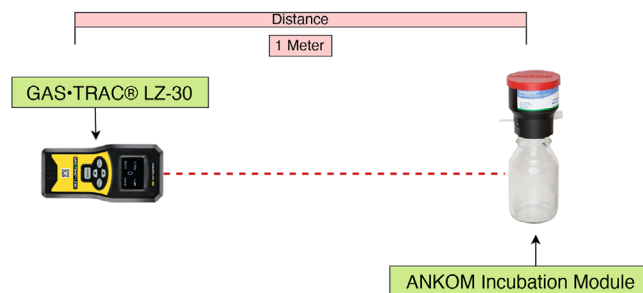


FIGURE 1 Schematic overview of using laser methane detector to read CH_4 emission values from ANKOM incubation module.

TABLE 2 GC data range classes, dataset distribution, and color modes.

Class	GC Range (ppm)	Train	Test	Validation	Color Modes
Class-1	166–171	1079	133	138	White hot, black hot, rainbow
Class-2	300–334	1268	157	162	White hot, black hot, rainbow
Class-3	457–510	1558	194	196	White hot, black hot

The CH_4 gas is generated from rumen liquor through a continuous culture fermenter system, which simulates the cow rumen environment. The gas is generated in 15 ANKOM incubation modules, with each module corresponding to one of the dietary treatments as described in Section 2.1. To ensure measurement accuracy within the optimal detection range of 0.5 m to 30 m, we place the detector 1 m away from each ANKOM incubation module, as shown in Figure 1, and record 100 readings for each module. All measurements were conducted at a controlled room temperature of 22°C , well within the device's optimal operating temperature range of -20°C to 45°C , ensuring stable and reliable detection performance.

Data collection was performed using a mobile application interface (SMART-LINK LIVE) connected to the GAS · TRAC® LZ-30 detector. This software interface allowed continuous monitoring of the target while simultaneously recording measurements. The data was exported from the mobile device for subsequent analysis.

3.2 | Dataset collection and optical gas imaging

We present the CD dataset, captured using the FLIR GF77 OGI camera, for the purpose of CH_4 plume detection and quantification. The dataset consists of CH_4 gas collected from a continuous culture fermenter system described in Section 2.1, which simulates the cow rumen environment. The CD dataset is divided into three classes based on the GC data ranges: Class-1 (166–171 ppm), Class-2 (300–334 ppm), and Class-3 (457–510 ppm) as shown in Table 2. These classes correspond to the CH_4 gas concentrations produced by the control diet, LF diet,

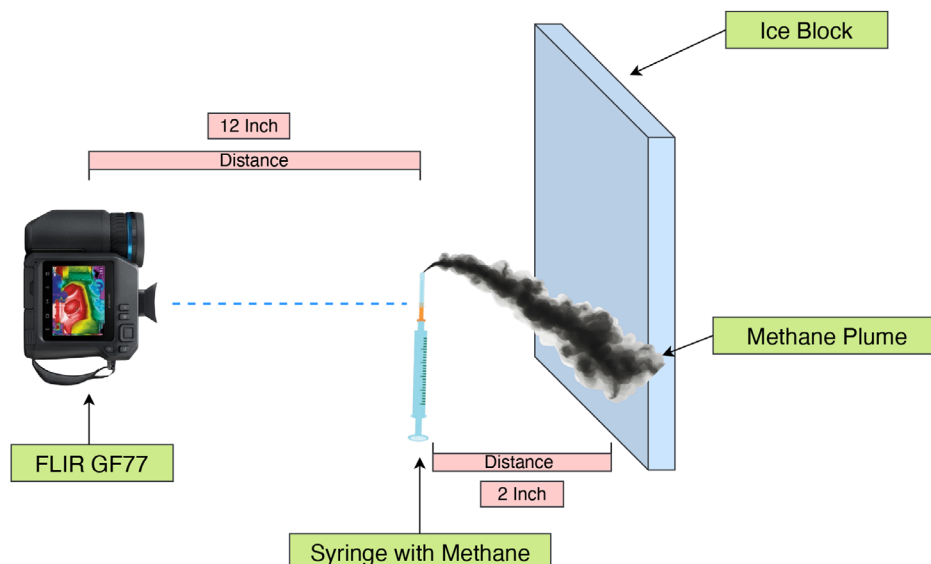


FIGURE 2 Schematic overview of using FLIR GF77 OGI camera to collect CH_4 plume images.

and HF diet, respectively. The CBR diet is excluded from the dataset due to its very low CH_4 concentration, which is below the detection limit of the OGI camera.

The FLIR GF77 camera uses an uncooled microbolometer detector with 320×240 pixel resolution and operates in the spectral range of $7\text{--}8.5\ \mu\text{m}$, optimized for CH_4 's absorption band at $7.7 \pm 0.1\ \mu\text{m}$. The camera's thermal sensitivity is $<25\ \text{mK}$ (NETD), with a minimum Noise Equivalent Concentration Length (NECL) of $100\ \text{ppm}\cdot\text{m}$ for CH_4 detection at a 1-m distance when maintaining a 10°C temperature differential. To effectively detect CH_4 plumes, a temperature difference of at least 3°C between the CH_4 plume and the background environment is required.

While high-end cooled-filter OGI cameras are typically used for detecting low-concentration CH_4 emissions from ruminants, we faced budget constraints that led us to explore alternative solutions with the more cost-effective uncooled FLIR GF77. Though the GF77 was primarily designed for industrial emission detection rather than low-concentration ruminant CH_4 emissions, we developed a novel imaging setup using a block of ice as the background, as shown in Figure 2. We tested the camera with air, CO_2 , and H_2 and found that the camera was not able to detect them with the same condition with the ice as the background.

Following the validation of our imaging setup, the CH_4 gas is transferred from the TEDLAR gas bags to syringes before release. Prior to releasing the gas, we record 15-s videos, which are later used for background removal. For each of the three GC data range classes, we capture three videos using the OGI camera, resulting in a total of nine videos. The camera is positioned 12 inches away from the syringe containing the CH_4 gas, while the syringe is placed 2 inches from the background. Frames are extracted from the captured videos to create the CD dataset, which consists of 4885 images with a resolution of 640×480 pixels. Samples of the collected images are shown in the first row in Figure 3. The CD dataset is then split into training, testing,

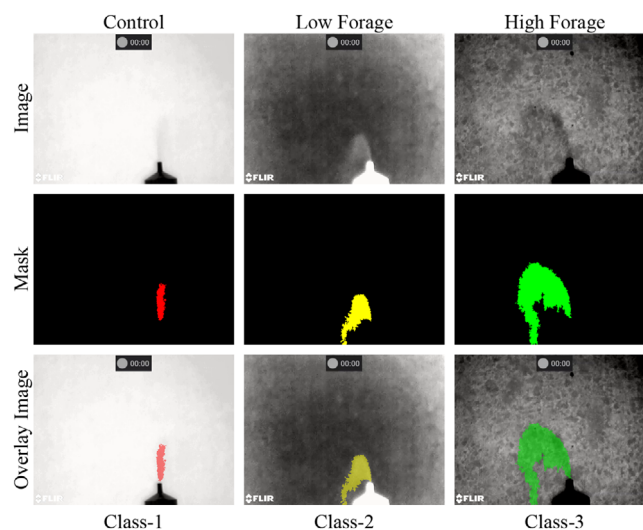


FIGURE 3 CH_4 plume visualization across different GC data range classes (Class-1: 166–171 ppm, Class-2: 300–334 ppm, and Class-3: 457–510 ppm) using the FLIR GF77 camera. The first row shows the original infrared images, the second row presents the corresponding ground truth masks, and the third row displays the overlay images, which are the ground truth masks superimposed on the original infrared images.

and validation subsets using an 80%, 10%, and 10% split ratio, respectively. Table 2 summarizes the GC data range classes, the dataset distribution, and the color modes used during video capture for the CD dataset.

3.3 | Mask generation

To generate labeled data for semantic segmentation tasks, we use a multi-step approach that begins with isolating CH_4 plumes from the foreground images through background subtraction. We achieve this by calculating an average image from the

TABLE 3 GC data ranges mapped to classes and corresponding diets.

Class	GC range (ppm)	Corresponding diet
Class-1	166–171	Control
Class-2	300–334	Low forage
Class-3	457–510	High forage

background frames captured before each gas release and subtracting it from the corresponding foreground frames. Next, we apply contrast enhancement techniques to the resulting images to improve the visibility of the CH₄ plumes, followed by an adaptive thresholding algorithm to convert the preprocessed images into a binary representation, effectively separating the CH₄ plumes from the background. To further refine the segmentation and precisely delineate the boundaries of the CH₄ plumes, we use the watershed algorithm [33], which is guided by an elevation map generated using a Sobel filter.

After obtaining the segmented objects, we perform region properties analysis to identify and assess each object individually. We select objects that exceed a predetermined size threshold for annotation while filtering out objects other than CH₄ plumes and smaller, insignificant objects. This ensures that we consider only gas plumes for the subsequent mask generation process. In the final step, we generate binary masks for each identified CH₄ plume, providing pixel-wise annotations that are crucial for training and evaluating semantic segmentation models, and we save the binary masks as separate images as shown in Figure 3. The classes identified from the GC data ranges, as shown in Table 3, represent different concentration ranges of CH₄ produced by the control, LF, and HF diets.

3.4 | Statistical analysis

To ensure the reliability and significance of our collected data, we performed comprehensive statistical analyses on both the in vitro experimental results and the laser detection measurements.

3.4.1 | In vitro data statistical analysis

The effect of different types of diet on enteric CH₄ emissions and rumen fermentation characteristics was determined using one-way analysis of variance (ANOVA) with JMP® Pro V17.2.0 statistical analysis software (SAS Institute, Cary, NC, USA). The diet type represented the fixed effect, and the replicates reflected the random effect. Student's t-test and Dunnett's test were used to analyze the p-values for all possible pairwise comparisons of the least square means (LSMEANS), and the significance was determined at a p-value less than 0.05.

3.4.2 | Laser data log statistical analysis

In this study, cleaning and preprocessing steps were implemented using IBM SPSS® statistics software version 29 to

improve the quality and accuracy of the data before further analysis. An explorative analysis of the descriptive statistics technique was implemented to investigate the features and detect the overall pattern of the dataset, including measures of central tendency and variability, such as mean, 95% confidence interval for the mean, variance, standard deviation, minimum, maximum, and range, as well as distribution. Extreme values with the highest and lowest cases and values were identified and removed as they could skew the analysis and distort the results. Normality tests were conducted using Shapiro-Wilk [34] to establish that the data follows a normal distribution, which is important for statistical analyses and sampling selection approaches. Moreover, a lower standard error of means and standard deviation was considered when selecting the best sample to ensure that the data was more reliable and consistent.

4 | GASFORMER ARCHITECTURE

While our previous work on Gasformer [16] focused on developing a semantic segmentation model for detecting CH₄ emissions at low flow rates (10–100 SCCM) and from dairy cow rumen gas samples, the present study extends this framework to quantify CH₄ emissions under different dietary treatments. In the original Gasformer article, we evaluated the model's performance on two distinct datasets: a Controlled Methane Release (MR) dataset with varying flow rates and a limited Dairy Cow Rumen Gas (CR) dataset of 340 images. The current study specifically applies and validates the Gasformer architecture on a new, comprehensive Controlled Diet (CD) dataset that correlates CH₄ concentrations with different dietary interventions (166–171 ppm for control diet, 300–334 ppm for LF diet, and 457–510 ppm for HF diet). This application represents a novel use of computer vision techniques in livestock CH₄ monitoring by directly linking visual plume characteristics to specific dietary impacts on CH₄ production, thereby providing a practical tool for evaluating feeding strategies aimed at reducing CH₄ emissions.

The Gasformer architecture, as illustrated in Figure 4, is based on an encoder-decoder architecture that leverages the Mix Vision Transformer (MiT) [35] as the encoder and a lightweight and efficient decoder called Light-Ham [36, 37].

4.1 | Encoder

The MiT encoder generates multi-scale feature representations from the input image without requiring explicit positional encoding. It uses an overlapped patch embedding operation to extract patches from the input image with 1/4 the spatial resolution of the input image denoted as F1 in the Figure 4 and a hierarchical stack of Transformer blocks to process the patch embeddings at different spatial resolutions. Each Transformer block consists of Efficient Self-Attention, Mix-FFN, and Overlapped Patch Merging components.

Within each Transformer block, an Efficient Self-Attention layer calculates the attention weights between patches using

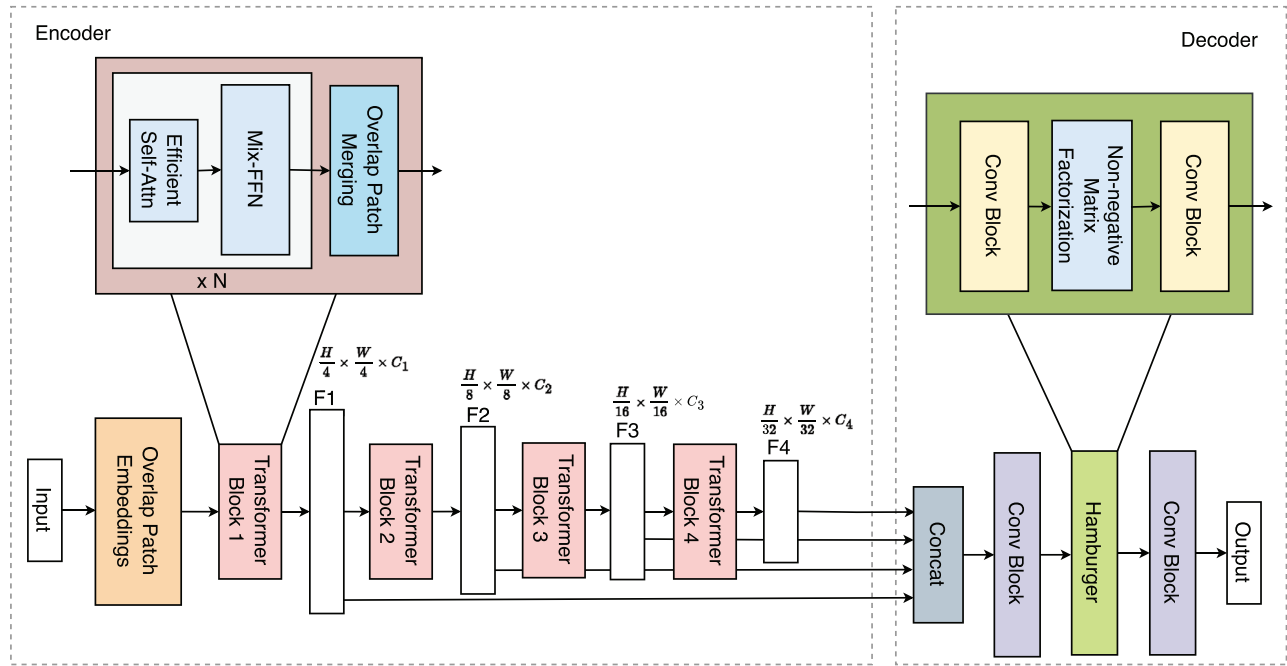


FIGURE 4 Overview of the Gasformer [16] architecture. The encoder is based on the Mix Vision Transformer, which extracts hierarchical feature representations (F1, F2, F3, F4) at different scales ($1/4$, $1/8$, $1/16$, $1/32$ of the original image resolution) from the input image. These features are then fed into the Light-Ham decoder, which leverages Hamburger Matrix Decomposition to capture long-range dependencies and produce the final segmentation output.

multi-head self-attention, projecting the patch embeddings into query, key, and value matrices. This allows the model to weigh the importance of different image regions when generating feature representations. To reduce computational complexity, a sequence reduction process [38] is applied, decreasing the self-attention computation from $O(n^2)$ to $O(n^2/r)$ where r is the reduction ratio. The encoder also incorporates a Mix-FFN block, which eliminates the need for traditional positional encoding by incorporating a 3×3 depth-wise convolution into the feed-forward network, capturing channel-specific spatial relationships. The Overlap Patch Merging operation is applied after each Transformer block stage and downsamples the feature maps while increasing the channel dimension, and generates multi-scale representations with resolutions of $1/8$, $1/16$, and $1/32$ of the input image size. These multi-scale features denoted as F2, F3, and F4 in the Figure 4, capture both local and global context.

4.2 | Decoder

The Light-Ham decoder takes multiple feature maps (F1, F2, F3, and F4) from different levels of the encoder as input. The feature maps are resized to have the same dimension as F1 and then concatenated to aggregate information from various scales.

A key component of the decoder is the Hamburger Matrix Decomposition [39] module. This module efficiently captures long-range dependencies by performing matrix decomposition using Non-negative Matrix Factorization as an alternative to self-attention. By factorizing the input features, the Hamburger module allows for a more compact and efficient representa-

tion of the global image context. The Light-Ham decoder also includes a squeeze layer to reduce the channel dimensions of the input feature maps and an alignment layer to match the output dimensions of the Hamburger module to the desired segmentation mask size.

4.3 | Model training

To classify and segment the CH_4 plume based on the diet, we use six semantic segmentation models: FCN [26], U-Net [23], DeepLabv3+ [27], Vision Transformer [28], Swin Transformer [29] and Gasformer [16]. We train the deep learning models using Pytorch [40] and MMsegmentation [41] on an Intel Core i9 11900F CPU (2.50GHz) with 32 GB of memory and an NVIDIA RTX 3090 graphics card. The encoders of FCN, DeepLabv3+, Vision Transformer, Swin Transformer and Gasformer are pre-trained on the ImageNet [42] dataset, while the encoder of Unet is pre-trained on the CityScapes [43] dataset.

We train each model for 160,000 iterations using AdamW [44] as an optimizer with a learning rate of 0.00006 and a weight decay of 0.01. To decay the learning rate, we employ a two-stage learning rate scheduler strategy: Linear learning rate for the first 1500 iterations and Polynomial learning rate for the remaining iterations. The batch sizes for train, test, and validation data are set to 2, 1, and 1, respectively. Every 16,000 iterations, we validate the models using the validation data and save the model's weights if there is an improvement in the mIoU score.

To prevent overfitting on the training dataset, we apply data augmentation techniques during training. We resize the images and the corresponding segmentation masks to a resolution of

TABLE 4 Effects of different diet treatment on gas production and rumen fermentation characteristics.

Parameter	Control	Control + Bromoform	High forage	Low forage	SEM [†]	<i>p</i> -value
CH ₄ (ppm)	167.22 ^c	1.41 ^d	482.45 ^a	293.72 ^b	17.180	0.001 [‡]
CO ₂ (%)	325.52	296.76	314.54	325.63	10.780	0.276
H ₂ (%)	2.90 ^b	29.96 ^a	3.14 ^b	3.24 ^b	1.023	0.001 [‡]
Total gas (mL)	382.82 ^a	327.98 ^b	374.10 ^a	384.17 ^a	13.046	0.027 [‡]
pH	6.64 ^b	6.57 ^c	6.80 ^a	6.31 ^d	0.009	0.001 [‡]
Ammonia (mg/dL)	9.78 ^c	4.22 ^d	32.83 ^a	20.87 ^b	0.314	0.001 [‡]
Total VFA (mmol)	63.57 ^b	62.03 ^{b,c}	58.33 ^c	70.16 ^a	1.697	0.001 [‡]
Acetate (C2) (mmol)	23.12 ^a	15.75 ^c	20.87 ^b	20.72 ^b	0.525	0.001 [‡]
Propionate (C3) (mmol)	17.38 ^b	21.71 ^a	14.34 ^c	21.07 ^a	0.532	0.001 [‡]
Butyrate (mmol)	14.84 ^b	12.17 ^c	12.74 ^c	18.98 ^a	0.543	0.001 [‡]
Iso-butyrate (mmol)	1.00 ^b	0.74 ^c	1.32 ^a	1.09 ^b	0.083	0.001 [‡]
Valerate (mmol)	4.79 ^c	9.70 ^a	6.12 ^b	5.46 ^{b,c}	0.298	0.001 [‡]
Iso-Valerate (mmol)	2.41 ^b	1.94 ^c	2.92 ^a	2.82 ^a	0.215	0.001 [‡]
C2:C3 ratio	1.33 ^b	0.72 ^d	1.45 ^a	0.98 ^c	0.035	0.001 [‡]

[†]SEM, Standard error of the mean; while the number of replicates or modules (*n*) = 3 – 4.

[‡]*p*-value < 0.05 indicates statistical significance at 95% confidence level.

^{a,b,c}Values with “a” are highest, followed by “b”, “c”, and “d” in descending order. Shared superscripts (e.g. bc) indicate values not distinctly different from either “b” or “c” but lower than “b” alone.

512 × 512 pixels with a ratio range of 0.5–2.0, randomly crop the image to a resolution of 512 × 512 pixels, and perform random horizontal flips. During testing and validation, we resize the images to a resolution of 512 × 512 pixels while maintaining their aspect ratios, without applying any other data augmentation techniques.

5 | RESULTS

5.1 | In vitro batch results

This article investigated the possibility of detecting and quantifying enteric CH₄ in vitro using LMD and OGI. The continuous culture and batch culture in vitro techniques were used for data collection and for data verification through GC instrument. The GC results in Table 4 for CH₄ showed that different diet types had a significant effect on CH₄. The HF diet had the highest CH₄ concentration, while the bromoform diet had traces of CH₄. The LF diet produced more CH₄ compared to the control (*p* < 0.01). There was no difference in the total gas values except for the CBR treatment, and no difference was recorded for CO₂ concentration. However, H₂ was higher in the bromoform treatment than in all other treatments (*p* < 0.01). The HF treatment had the highest pH value, while the LF treatment had the lowest pH value (*p* < 0.01). NH₃-N concentration was higher in the HF, followed by LF, while the CBR diet had the lowest NH₃-N compared to all treatments (*p* < 0.01). The LF treatment had the highest total VFA concentration, while HF had the lowest compared to Control and CBR (*p* < 0.01). The molar proportion of acetate was also significantly different among treatments. The CBR diet had the lowest acetate concentration,

TABLE 5 LMD readings in ppm-m.

Diet treatment	Mean	Std. error	95% Confidence interval		Std. deviation
			Lower bound	Upper bound	
Control	3105.13 ^b	9.63	3086.2	3124.06	190.68
CBR	74.98 ^c	3.26	68.57	81.39	58.196
HF	9594.41 ^a	34.87	9525.89	9662.92	786.02
LF	3057.22 ^b	16.5	3024.77	3089.67	313.5

^{a,b,c}Values with a are highest, followed by b, and c in descending order.

while the control treatment had the highest acetate concentration (*p* < 0.01). No significant difference was observed between LF and HF for the acetate concentration. LF and CBR had the highest propionate molar concentration, while HF had the lowest propionate molar concentration (*p* < 0.01). LF had the highest butyrate molar concentration, while HF, and CBR had the lowest butyrate molar concentration (*p* < 0.01). Iso-valerate was lower in the CBR than all other treatments (*p* < 0.01). The HF had the highest acetate to propionate ratio, while the CBR treatment had the lowest ratio compared to control (*p* < 0.01).

5.2 | Laser methane detector results

LMD readings are shown in Table 5. Results showed that HF treatment had the highest CH₄ concentration (*p* < 0.01) compared with all treatments. There was no difference in CH₄ concentration between the control and LF treatments. The CBR diet had the lowest CH₄ reading compared to all treatments

TABLE 6 Test of normality of CH₄ concentrations in ppm-m using Shapiro-Wilk for LMD readings.

Diet treatment	Statistic	df	Sig.
Control	0.911	392	<.001
CBR	0.883	319	<.001
HF	0.978	508	<.001
LF	0.957	361	<.001

TABLE 7 Performance comparison of semantic segmentation architectures on CH₄ plume segmentation task.

Architecture	Image size	mIoU ↑	mFscore ↑
FCN	512 × 512	84.02	91.04
U-Net	512 × 512	82.02	89.7
Vision transformer	512 × 512	55.69	67.9
Swin transformer	512 × 512	83.97	91.02
DeepLabv3+	512 × 512	84.49	91.33
Gasformer	512 × 512	85.1	91.72

($p < 0.01$). The test of normality results are shown in Table 6. All treatments followed a normal distribution ($p < 0.01$).

5.3 | Optical gas imaging results

5.3.1 | Quantitative comparisons

Table 7 presents the performance comparison of six semantic segmentation architectures, namely FCN, U-Net, DeepLabv3+, Vision Transformer, Swin Transformer and Gasformer, on the task of CH₄ plume segmentation. All models are trained and evaluated using an input image size of 512 × 512 pixels. The evaluation metrics used are mIoU and mFscore, which are widely adopted in semantic segmentation tasks [23, 26]. Among the six architectures, Gasformer achieves the highest performance with a mIoU of 85.1% and a mFscore of 91.72%. This indicates that Gasformer is able to accurately segment the CH₄ plume regions while maintaining high precision and recall. The superior performance of Gasformer can be attributed to its ability to generate multi-scale feature representations from the input image without explicit positional encoding and its use of the Mix-FFN block, which incorporates a 3 × 3 depth-wise convolution to encode local spatial relationships directly into the feature representations [35].

DeepLabv3+ and FCN also demonstrate strong performance, with mIoU scores of 84.49% and 84.02%, respectively. These models incorporate multi-scale contextual information through their atrous spatial pyramid pooling [45] and skip connections [46], respectively. However, their mFscore is slightly lower compared to Gasformer, suggesting a higher number of false positive or false negative predictions. The Swin Transformer achieves an mIoU of 83.97% and an mFscore of 91.02%, demonstrating its effectiveness in capturing both local and global context information through its hierarchical architecture and shifted window attention mechanism [29].

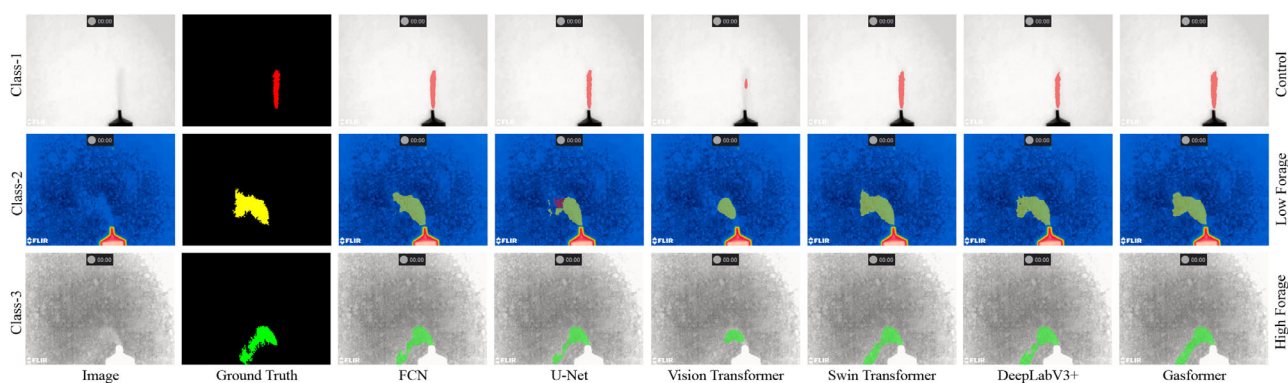
U-Net achieves an mIoU of 82.02% and an mFscore of 89.7%. Although U-Net has been widely used in medical image segmentation tasks [23, 47], its performance on the CH₄ plume segmentation task across different GC data range classes is lower than all architectures except Vision Transformer. This could be due to its limited ability to capture long-range dependencies and global context information. The Vision Transformer exhibits the poorest performance among the six architectures, with an mIoU of 55.69% and an mFscore of 67.9%. This can be attributed to the Vision Transformer's lack of inductive bias, which makes it more data-hungry and less suitable for tasks with limited training data [28].

Table 8 presents a detailed performance analysis of the six semantic segmentation models on the CH₄ plume segmentation task, evaluating them on four different classes: Background, Class-1, Class-2, and Class-3. The evaluation metrics used are Intersection over Union (IoU) and F-score, providing a comprehensive assessment of the models' segmentation accuracy. All models achieve high IoU and F-score values for the background class, with Gasformer and DeepLabv3+ slightly outperforming FCN, U-Net, Vision Transformer, and Swin Transformer, indicating their capability to accurately distinguish the background regions from the CH₄ plumes. For Class-1, Gasformer achieves the highest IoU and F-score, followed by Swin Transformer and DeepLabv3+, while Vision Transformer shows significantly lower performance. In Class-2, Gasformer maintains its lead, followed by DeepLabv3+ and Swin Transformer, while FCN, U-Net, and Vision Transformer lag behind. Although FCN achieves the highest IoU and F-score for Class-3, Gasformer, and DeepLabv3+ still exhibit strong performance, demonstrating their robustness across different CH₄ concentration levels. The Swin Transformer demonstrates competitive performance across all classes, while the Vision Transformer struggles to accurately segment the plumes, particularly in Class-1, where it achieves the lowest scores among all evaluated models.

Table 9 presents a computational efficiency analysis of the six semantic segmentation architectures, considering FPS on GPU, GFlops, and the number of parameters in millions (Params (M)). Gasformer achieves the highest FPS of 64.5, demonstrating its superior real-time performance compared to the other architectures. It is 1.26x faster than FCN, 1.37x faster than U-Net, 2.21x faster than Swin Transformer, 2.84x faster than Vision Transformer, and 1.40x faster than DeepLabv3+. This can be attributed to its efficient self-attention mechanism and the use of the Mix-FFN block, which allows for parallel computation and reduces the computational overhead [35]. Gasformer also has the lowest GFlops value of 9.92, indicating its computational efficiency, requiring 19.96x, 20.46x, 23.79x, 44.63x and 17.74x fewer GFlops compared to FCN, U-Net, Swin Transformer, Vision Transformer, and DeepLabv3+, respectively. In terms of model size, Gasformer is the most parameter-efficient among the six architectures, with only 3.65 million parameters. Gasformer is 12.92x smaller than FCN, 7.94x smaller than U-Net, 16.15x smaller than Swin Transformer, 38.9x smaller than Vision Transformer, and 11.29x smaller than DeepLabv3+. This makes Gasformer suitable for deployment on resource-constrained devices or scenarios with limited memory. The computational efficiency analysis highlights the

TABLE 8 Class-wise performance analysis of semantic segmentation models on CH₄ plume segmentation task.

Architecture	IoU				F-score			
	Background ↑	Class-1↑	Class-2↑	Class-3↑	Background ↑	Class-1↑	Class-2↑	Class-3↑
FCN	99.6	74.48	79.55	82.47	99.8	85.37	88.61	90.39
U-Net	99.56	67.68	79.54	81.3	99.78	80.73	88.6	89.68
Vision transformer	98.95	24.89	46.95	51.95	99.47	39.86	63.9	68.38
Swin transformer	99.59	74.86	80.21	81.21	99.8	85.62	89.02	89.63
DeepLabv3+	99.61	74.79	81.33	82.21	99.81	85.58	89.71	90.24
Gasformer	99.62	76.94	82.31	81.51	99.81	86.97	90.3	89.81

**FIGURE 5** Segmentation performance of different models on CD dataset, showing the input images, ground truth masks, and the segmentation outputs for Class-1 (166–171 ppm), Class-2 (300–334 ppm), and Class-3 (457–510 ppm).**TABLE 9** Computational efficiency analysis of semantic segmentation architectures on CH₄ plume segmentation task.

Architecture	FPS ↑	GFlops ↓	Params (M) ↓
FCN	51.37	198	47.125
U-Net	47.09	203	28.987
Vision transformer	22.72	443	142
Swin transformer	29.26	236	58.943
DeepLabv3+	46.2	176	41.217
Gasformer	64.56	9.921	3.65

trade-offs between real-time performance, computational complexity, and parameter efficiency, with Gasformer emerging as the most efficient architecture, achieving the highest FPS with the lowest GFlops and parameter count.

5.3.2 | Qualitative comparison

Figure 5 presents a qualitative comparison of the segmentation models' performance on three different GC data range classes: Class-1, Class-2, and Class-3. The results demonstrate that all segmentation models except the Vision Transformer perform well when the contrast between the gas plume and the background is high and the gas plume shape is simple, as observed

in the Class-1 case. However, the models exhibit varying levels of performance when faced with more challenging scenarios, such as complex gas plume shapes or low contrast between the gas plume and the background.

In the Class-2 case, where the contrast between the gas plume and the background is low, the models face difficulties in accurately predicting the mask. The U-Net model, in particular, exhibits suboptimal performance in this scenario, not only misclassifying the plume but also failing to predict the complete shape of the gas plume. The Vision Transformer demonstrates significant limitations, failing to accurately segment the plume and missing substantial portions of its structure. In contrast, the Gasformer model demonstrates its robustness by correctly classifying and predicting the shape of the plume despite the challenging low-contrast conditions. Similarly, in the Class-3 case, where the gas plume shape is complex, the Gasformer model stands out as the only architecture capable of completely and accurately predicting the segmentation mask. The other models struggle to capture the intricate details of the plume's shape, resulting in incomplete or inaccurate segmentation.

6 | DISCUSSION

Our approach to CH₄ detection using an ice background represents a departure from traditional OGI techniques, which typically rely on infrared spectral absorption characteristics

where gases absorb background radiation to create visible plumes. While this modified method makes the ruminant-discharged gas a thermal target, primarily showing its radiation characteristics, we validated its effectiveness through rigorous testing. Controlled experiments demonstrated that the FLIR GF77, despite lacking the cooled filter found in more expensive OGI systems, could selectively detect CH₄ while showing no response to other gases such as CO₂ and H₂ under identical conditions. This validation, combined with our GC data correlation, supports the reliability of our modified approach for CH₄-specific detection in low-concentration scenarios.

Having established the validity of our detection methodology, it is important to distinguish the contributions of this work from our previous research. While our previous work on Gasformer [16] demonstrated the model's capability to detect CH₄ gas in daily cow rumen samples, the present study adapts this framework for diet-specific quantification. By modifying the model to handle three distinct classes corresponding to different CH₄ concentration ranges (166–171 ppm for control diet, 300–334 ppm for LF diet, and 457–510 ppm for HF diet), we enable automated assessment of dietary impacts on CH₄ emissions through visual analysis. This application of the Gasformer model to dietary intervention assessment represents a novel use case in livestock CH₄ monitoring.

While this study utilizes in vitro measurements rather than direct animal trials, our methodology is grounded in well-established practices for ruminant research. The ANKOM gas production system used in this study is a validated approach for simulating rumen fermentation and is widely accepted in the scientific community as a preliminary step before conducting more resource-intensive in vivo trials. The rumen liquid used in our experimental setup was collected directly from fistulated dairy cattle, ensuring that the microbial ecosystem closely represents actual rumen conditions. This in vitro approach allows for controlled experimentation and method validation while minimizing animal use and research costs.

Having established the scientific validity of our in vitro approach, the possibility of detecting and quantifying enteric CH₄ in vitro using LMD and OGI was investigated in this article. The in vitro batch culture data analysis for CH₄ and rumen fermentation parameters was conducted for two main reasons: the first reason is to establish a dataset collection source, which is the enteric CH₄ produced by the gas production modules that were used for imaging, while the second reason is to compare and validate the results of the OGI and the LMD with the lab techniques approved in peer-reviewed literature.

The F:C ratio is one of the strategies that have been investigated for enteric CH₄ mitigation. Increasing the F:C ratio was reported to increase the enteric CH₄ emission from dairy cows. Aguerre et al. [48] reported that increasing the F:C ratio in the diet of dairy cows from 47:53 to 68:32 increased CH₄ from 538 to 648 g/cow per day. The findings of this article are in agreement with our results, where increasing the F:C ratio from 20:80 to 80:20 increased CH₄ emission from 293.72 to 482.45. The same article also reported no changes in CO₂ which is also in agreement with our results. Bromoform, the active component in red seaweed *A. taxiformis*, was reported to inhibit CH₄ and

was used in this experiment as a negative control. The addition of bromoform at 0.14 µl/Liter of rumen fluid/day was able to inhibit CH₄ by 98% compared to control. These findings are in agreement with the findings of Roque et al. [49] indicated that adding *Asparagopsis armata* to lactating dairy cows' diet at two inclusion rates (0.5 and 1%) reduced CH₄ yield by 26.4 and 67.2%, respectively. H₂ concentrations were also high with adding bromoform compared to all treatments, which is attributed to bromoform's mode of action that targets the pathway of CH₄ formation, which results in a higher accumulation of H₂ [50–52]. Increasing the F:C ratio increased the pH inside the rumen culture while increasing the concentrated amount favors the acid-producing bacteria and the starch-producing bacteria that led to the formation of more H₂ and reduced the pH, while increasing the propionate production in the rumen culture, which was also noticed in this study. Aguerre et al. [48] reported that increasing the F:C ratio in the diet of dairy cows from 47:53 to 68:32 increased pH from 6.38 to 6.59, which is in agreement with the findings of this article, where increasing the F:C ratio increased pH from 6.31 to 6.8.

The LMD data followed the same pattern for the HF diet that had the highest CH₄ values, while LF values were less than the HF, and these results matched the GC results. The use of an LMD in quantifying enteric CH₄ was investigated by Chagunda et al. [4], who reported that the physiological status of the animal and the animal behavior could affect the released CH₄ from the animal. Chagunda reported that dairy cows produced more CH₄ when ruminating than when eating or sleeping. Another study by Chagunda [5] reported that the highest CH₄ values were recorded while drinking. From these findings, we can expect that the laser CH₄ readings will differ with different F:C ratios. However, the feasibility of using LMD for measuring enteric CH₄ was also investigated in these studies, and the daily CH₄ production was 357 g/day, which is considered 17% higher than the estimated through the mathematical equation based on the daily intake of dry matter.

OGI input for developing a deep learning model that can identify and quantify CH₄ is also investigated in the current article. The Gasformer model demonstrates significant performance in segmenting CH₄ plumes from the CD dataset, outperforming other state-of-the-art semantic segmentation architectures such as FCN, U-Net, Vision Transformer, Swin Transformer, and DeepLabv3+. The qualitative comparison of CH₄ plume visualization across different GC data range classes highlights the Gasformer model's ability to accurately segment plumes with varying shapes and intensities. This is particularly evident in the Class-2 and Class-3 cases, where the model successfully captures low-contrast scenarios and complex plume shapes, respectively. The Gasformer model's computational efficiency, as demonstrated by its high FPS, low GFlops, and minimal parameter count, makes it well-suited for real-time applications and deployment on resource-constrained devices.

OGI, coupled with deep learning models like Gasformer, presents a promising alternative solution for detecting and quantifying CH₄ emissions from livestock. Unlike traditional methods such as gas chambers or LMD, OGI allows for non-invasive measurements and provides high spatial and temporal

resolution. The ability to visualize and analyze CH₄ plumes in real-time using OGI and deep learning algorithms offers a more comprehensive understanding of the emission patterns and distribution, which can aid in developing targeted mitigation strategies. Furthermore, the portability and flexibility of OGI systems make them suitable for on-site measurements and monitoring, enabling a more practical approach to assessing CH₄ emissions from livestock in various settings.

The Gasformer model's ability to provide non-invasive measurements and high spatial and temporal resolution is based on the infrared images captured by the FLIR GF77 camera. However, it is important to note that the camera still needs to be positioned in close proximity to the emission source to effectively detect and visualize the CH₄ plumes, similar to the GAS · TRAC® LZ-30 LMD. The key difference is that the Gasformer model analyzes the infrared images to provide a more comprehensive understanding of the plume dynamics and distribution, while the GAS · TRAC® detector provides point measurements of CH₄ concentrations.

However, it is essential to acknowledge the limitations of the Gasformer model and the CD dataset. The controlled laboratory setting in which the dataset is collected may not fully represent the complexity and variability of real-world CH₄ emissions from livestock. Additionally, the limited number of GC data range classes and the quantity of data collected for each treatment may impact the model's ability to generalize to new, unseen data or plumes from livestock under different dietary treatments.

To address these limitations and further enhance the Gasformer model's capabilities, future work should focus on expanding the dataset to include a wider range of GC data range classes and collecting more extensive data for each class. This would enable the development of more robust and generalizable models capable of accurately segmenting CH₄ plumes across a broader spectrum of CH₄ concentrations. Validating the model's performance on real-world data collected from actual livestock emissions is also crucial to assess its practical applicability and identify potential challenges in real-world deployment.

To advance this validation further, we plan to conduct in vivo experiments to collect CH₄ emission data directly from ruminants. This future work will involve capturing OGI data from live cattle under different dietary treatments, allowing us to evaluate how well our model's performance on in vitro data translates to actual livestock emissions. The in vivo dataset will help bridge the gap between laboratory conditions and practical farm applications while potentially revealing new challenges and opportunities for CH₄ detection in real farming environments. This extension to live animal studies represents a critical next step in establishing the practical utility of our OGI and deep learning approach for livestock CH₄ monitoring.

The methodologies used in this study, particularly the use of OGI and deep learning models like Gasformer, have the potential to be applied to the quantification of other greenhouse gases, such as CO₂ and N₂O. However, detecting these gases would require cameras with different lenses, such as the FLIR G343 for CO₂ quantification. By developing effective tools to detect

and quantify various greenhouse gases, researchers and policy-makers can gain valuable insights into the impact of livestock production on global climate change. This information can be used to develop targeted strategies and legislation for better management practices and animal health, ultimately mitigating the impact of livestock production on global warming. Future research should explore the adaptation of the current methodology to other greenhouse gases and investigate the potential for an integrated approach to monitoring and mitigating the environmental impact of livestock production.

Exploring data augmentation techniques, transfer learning approaches, or few-shot learning methods could help improve the model's ability to adapt to new GC data range classes or limited data scenarios. Furthermore, establishing a direct quantitative relationship between the Gasformer model's output and the GAS · TRAC® detector's measurements would enhance the model's utility in providing absolute concentration measurements, facilitating a more comprehensive understanding of CH₄ emissions from livestock under different dietary conditions.

7 | CONCLUSIONS

This research demonstrates the potential of integrating computer vision, deep learning, OGI, and LMD techniques for precise and non-invasive monitoring of enteric CH₄ emissions from livestock. We introduced the CD dataset captured using a FLIR GF77 OGI camera, which includes a diverse range of CH₄ plumes across different gas chromatography data range classes. The previously published Gasformer architecture, a transformer-based semantic segmentation architecture, outperforms state-of-the-art models such as FCN, U-Net, Vision Transformer, Swin Transformer, and DeepLabv3+ on the CD dataset. The model's superior performance in detecting and quantifying CH₄ emissions can be attributed to its ability to effectively capture complex plume shapes and low-contrast scenarios while maintaining high computational efficiency. These findings have important practical applications for optimizing feeding management practices. By combining OGI technology with the Gasformer model, livestock farmers can establish an early detection system that provides valuable insights into the impact of management practices, such as animal intensification and dietary choices. This information enables farmers to make informed decisions to adjust their feeding strategies and minimize environmental impact. Our investigation of the GAS · TRAC® LZ-30 LMD to measure CH₄ concentrations from the ANKOM incubation modules shows that LMD measurements follow a similar pattern to the GC results, validating its viability for quantifying emissions under different dietary treatments. The integration of non-invasive OGI and supplementary LMD techniques provides a comprehensive monitoring approach that enables the development of targeted mitigation strategies. Future work should focus on expanding the dataset, validating the model's performance on real-world livestock emissions data, and exploring data augmentation, transfer learning, and few-shot learning methods to enhance adaptability. By addressing these limitations and

further refining the models, these techniques could contribute to developing effective quantification strategies and sustainable livestock production practices, ultimately mitigating the environmental impact of CH₄ emissions.

AUTHOR CONTRIBUTIONS

Mohamed G. Embaby: Conceptualization; methodology; formal analysis; investigation; data curation; writing—original draft. **Toqi Tahamid Sarker:** Conceptualization; software; formal analysis; investigation; data curation; writing—original draft; visualization. **Amer AbuGhazaleh:** Conceptualization; methodology; resources; writing—review & editing; supervision; project administration; funding acquisition. **Khaled R. Ahmed:** Conceptualization; methodology; validation; resources; writing—original draft; writing—review & editing; supervision; project administration; funding acquisition.

ACKNOWLEDGEMENTS

The authors thank Siraj O. Mohammed for his assistance with the statistical analysis.

This research was supported by the National Institute of Food and Agriculture, United States Department of Agriculture, under Award Number 2022-70001-37404, and the Office of the Vice Chancellor for Research at Southern Illinois University Carbondale.

CONFLICT OF INTEREST STATEMENT

The authors declare no conflicts of interest.

DATA AVAILABILITY STATEMENT

The data that support the findings of this study are available from the corresponding author upon reasonable request.

ORCID

Toqi Tahamid Sarker  <https://orcid.org/0000-0003-2482-8059>

REFERENCES

- US EPA, OAR. Understanding global warming potentials (2016). <https://www.epa.gov/ghgemissions/understanding-global-warming-potentials>
- Beauchemin, K.A., Ungerfeld, E.M., Eckard, R.J., Wang, M.: Fifty years of research on rumen methanogenesis: Lessons learned and future challenges for mitigation. *Animal* 14(S1), s2–s16 (2020)
- Hook, S.E., Wright, A.D.G., McBride, B.W.: Methanogens: Methane producers of the rumen and mitigation strategies. *Archaea* 2010, 945785 (2010)
- Chagunda, M., Ross, D., Roberts, D.: On the use of a laser methane detector in dairy cows. *Comput. Electron. Agric.* 68(2), 157–160 (2009)
- Chagunda, M.: Opportunities and challenges in the use of the laser methane detector to monitor enteric methane emissions from ruminants. *Animal* 7, 394–400 (2013)
- Ricci, P., Chagunda, M., Rooke, J., Houdijk, M.J., Duthie, C.A., Hyslop, J., et al.: Evaluation of the laser methane detector to estimate methane emissions from ewes and steers. *J. Anim. Sci.* 92(11), 5239–5250 (2014)
- Kumar, S., Torres, C., Ulutan, O., Ayasse, A., Roberts, D., Manjunath, B.: Deep remote sensing methods for methane detection in overhead hyperspectral imagery. In: *Proceedings of the IEEE/CVF Winter Conference on Applications of Computer Vision*, pp. 1776–1785. IEEE, Piscataway (2020)
- Kumar, S., Arevalo, I., Iftekhar, A., Manjunath, B.: Methanemapper: Spectral absorption aware hyperspectral transformer for methane detection. In: *Proceedings of the IEEE/CVF Conference on Computer Vision and Pattern Recognition*, pp. 17609–17618. IEEE, Piscataway (2023)
- Rouet Leduc, B., Hulbert, C.: Automatic detection of methane emissions in multispectral satellite imagery using a vision transformer. *Nat. Commun.* 15(1), 3801 (2024)
- Almalky, A.M., Ahmed, K.R.: Deep learning for detecting and classifying the growth stages of *consolida regalis* weeds on fields. *Agronomy* 13(3), 934 (2023)
- Sarker, T.T., Islam, T., Ahmed, K.R.: Cannabis seed variant detection using faster r-cnn. In: *10th IEEE International Conference on Advanced Computing and Communication Systems (ICACCS 2024)*. IEEE, Piscataway (2024)
- Goshika, S., Meksem, K., Ahmed, K.R., Lakhssassi, N.: Deep learning model for classifying and evaluating soybean leaf disease damage. *Int. J. Mol. Sci.* 25(1), 106 (2023)
- Oliveira, D.A.B., Pereira, L.G.R., Bresolin, T., Ferreira, R.E.P., Dorea, J.R.R.: A review of deep learning algorithms for computer vision systems in livestock. *Livestock Sci.* 253, 104700 (2021)
- Dhanya, V., Subeesh, A., Kushwaha, N., Vishwakarma, D.K., Kumar, T.N., Ritika, G., et al.: Deep learning based computer vision approaches for smart agricultural applications. *Artif. Intell. Agric.* 6, 211–229 (2022)
- Han, S., Fuentes, A., Yoon, S., Jeong, Y., Kim, H., Park, D.S.: Deep learning-based multi-cattle tracking in crowded livestock farming using video. *Comput. Electron. Agric.* 212, 108044 (2023)
- Sarker, T.T., Embaby, M.G., Ahmed, K.R., Abughazaleh, A.: Gasformer: A transformer-based architecture for segmenting methane emissions from livestock in optical gas imaging. In: *Proceedings of the IEEE/CVF Conference on Computer Vision and Pattern Recognition (CVPR) Workshops*, pp. 5489–5497. IEEE, Piscataway (2024)
- Ren, C., Kim, D.K., Jeong, D.: A survey of deep learning in agriculture: techniques and their applications. *J. Inf. Process. Syst.* 16(5), 1015–1033 (2020)
- Karami, H., Kamruzzaman, M., Covington, J.A., Hassouna, M., Darvishi, Y., Ueland, M., et al.: Advanced evaluation techniques: Gas sensor networks, machine learning, and chemometrics for fraud detection in plant and animal products. *Sens. Actuators A* 370, 115192 (2024)
- Jongaramrungruang, S., Thorpe, A.K., Matheou, G., Frankenberg, C.: Methanet—an ai-driven approach to quantifying methane point-source emission from high-resolution 2-d plume imagery. *Remote Sens. Environ.* 269, 112809 (2022)
- Ramirez Agudelo, J.F., Escobar Restrepo, C.S., Muñoz Tamayo, R., Posada Ochoa, S.L., Rosero Noguera, R.: Intake time as potential predictor of methane emissions from cattle. *agRxiv* (2022)
- Ultralytics. YOLOv5: A state-of-the-art real-time object detection system. <https://docs.ultralytics.com> (2021)
- Jeong, S., Fischer, M.L., Breunig, H., Marklein, A.R., Hopkins, F.M., Biraud, S.C.: Artificial intelligence approach for estimating dairy methane emissions. *Environ. Sci. Technol.* 56(8), 4849–4858 (2022)
- Ronneberger, O., Fischer, P., Brox, T.: U-net: Convolutional networks for biomedical image segmentation. In: *Medical Image Computing and Computer-Assisted Intervention—MICCAI 2015: 18th International Conference*, pp. 234–241. Springer, Cham (2015)
- Wang, J., Tchammi, L.P., Ravikumar, A.P., McGuire, M., Bell, C.S., Zimmerle, D., et al.: Machine vision for natural gas methane emissions detection using an infrared camera. *Appl. Energy* 257, 113998 (2020)
- Wang, J., Ji, J., Ravikumar, A.P., Savarese, S., Brandt, A.R.: Videogasnet: Deep learning for natural gas methane leak classification using an infrared camera. *Energy* 238, 121516 (2022)
- Long, J., Shelhamer, E., Darrell, T.: Fully convolutional networks for semantic segmentation. In: *Proceedings of the IEEE Conference on Computer Vision and Pattern Recognition*, pp. 3431–3440. IEEE, Piscataway (2015)
- Chen, L.C., Zhu, Y., Papandreou, G., Schroff, F., Adam, H.: Encoder-decoder with atrous separable convolution for semantic image segmentation. In: *Proceedings of the European Conference on Computer Vision (ECCV)*, pp. 801–818. Springer, Berlin (2018)
- Dosovitskiy, A.: An image is worth 16x16 words: Transformers for image recognition at scale. *arXiv preprint arXiv:2010.11929* (2020)

29. Liu, Z., Lin, Y., Cao, Y., Hu, H., Wei, Y., Zhang, Z., et al.: Swin transformer: Hierarchical vision transformer using shifted windows. In: Proceedings of the IEEE/CVF International Conference on Computer Vision, pp. 10012–10022. IEEE, Piscataway (2021)
30. Teather, R., Sauer, F.: A naturally compartmented rumen simulation system for the continuous culture of rumen bacteria and protozoa. *J. Dairy Sci.* 71(3), 666–673 (1988)
31. McDougall, E.: Studies on ruminant saliva: 1. The composition and output of sheep's saliva. *Biochem. J.* 43(1), 99 (1948)
32. Jenkins, T.: Effect of fats and fatty acid combinations on ruminal fermentation in semi-continuous *in vitro* cultures. *J. Anim. Sci.* 64(5), 1526–1532 (1987)
33. Beucher, S.: Watershed, hierarchical segmentation and waterfall algorithm. In: Mathematical Morphology and Its Applications to Image Processing, pp. 69–76. Springer, Dordrecht (1994)
34. Mishra, P., Pandey, C.M., Singh, U., Gupta, A., Sahu, C., Keshri, A.: Descriptive statistics and normality tests for statistical data. *Ann. Cardiac Anaesthesia* 22(1), 67–72 (2019)
35. Xie, E., Wang, W., Yu, Z., Anandkumar, A., Alvarez, J.M., Luo, P.: Segformer: Simple and efficient design for semantic segmentation with transformers. In: Advances in Neural Information Processing Systems, vol. 34, pp. 12077–12090. Curran Associates, Inc. (2021)
36. Guo, M.H., Lu, C.Z., Liu, Z.N., Cheng, M.M., Hu, S.M.: Light-Ham. (2021). https://github.com/Gsunshine/Enjoy-Hamburger/tree/main/seg_light_ham
37. Guo, M.H., Lu, C.Z., Liu, Z.N., Cheng, M.M., Hu, S.M.: Visual attention network. *arXiv preprint arXiv:220209741* (2022)
38. Wang, W., Xie, E., Li, X., Fan, D.P., Song, K., Liang, D., et al.: Pyramid vision transformer: A versatile backbone for dense prediction without convolutions. In: Proceedings of the IEEE/CVF International Conference on Computer Vision, pp. 568–578. IEEE, Piscataway (2021)
39. Geng, Z., Guo, M.H., Chen, H., Li, X., Wei, K., Lin, Z.: Is attention better than matrix decomposition?. In: International Conference on Learning Representations. IEEE Information Theory Society, Piscataway (2020)
40. Ansel, J., Yang, E., He, H., Gimelshein, N., Jain, A., Voznesensky, M., et al.: PyTorch 2: Faster machine learning through dynamic Python bytecode transformation and graph compilation. In: 29th ACM International Conference on Architectural Support for Programming Languages and Operating Systems, vol. 2 (ASPLOS '24). ACM, New York (2024). <https://pytorch.org/assets/pytorch2-2.pdf>
41. Contributors, M.: MMSegmentation: Openmmlab semantic segmentation toolbox and benchmark. <https://github.com/open-mmlab/mms Segmentation> (2020)
42. Deng, J., Dong, W., Socher, R., Li, L.J., Li, K., Fei Fei, L.: Imagenet: A large-scale hierarchical image database. In: 2009 IEEE Conference on Computer Vision and Pattern Recognition, pp. 248–255. IEEE, Piscataway (2009)
43. Cordts, M., Omran, M., Ramos, S., Rehfeld, T., Enzweiler, M., Benenson, R., et al.: The cityscapes dataset for semantic urban scene understanding. In: Proceedings of the IEEE Conference on Computer Vision and Pattern Recognition, pp. 3213–3223. IEEE, Piscataway (2016)
44. Loshchilov, I., Hutter, F.: Decoupled weight decay regularization. In: International Conference on Learning Representations. IEEE Information Theory Society, Piscataway (2018)
45. Chen, L.C., Papandreou, G., Kokkinos, I., Murphy, K., Yuille, A.L.: Deeplab: Semantic image segmentation with deep convolutional nets, atrous convolution, and fully connected crfs. *IEEE Trans. Pattern Anal. Mach. Intell.* 40(4), 834–848 (2017)
46. He, K., Zhang, X., Ren, S., Sun, J.: Deep residual learning for image recognition. In: Proceedings of the IEEE Conference on Computer Vision and Pattern Recognition, pp. 770–778. IEEE, Piscataway (2016)
47. Manoj, A., Ahmed, K.R., Omar, G.: Porosity prediction of 3d printed components using u-net and its variants. In: 3rd IEEE International Conference on Artificial Intelligence For Internet of Things (AlloT 2024). IEEE, Piscataway (2024)
48. Aguerre, M.J., Wattiaux, M.A., Powell, J., Broderick, G.A., Arndt, C.: Effect of forage-to-concentrate ratio in dairy cow diets on emission of methane, carbon dioxide, and ammonia, lactation performance, and manure excretion. *J. Dairy Sci.* 94(6), 3081–3093 (2011)
49. Roque, B.M., Salwen, J.K., Kinley, R., Kebreab, E.: Inclusion of asparagopsis armata in lactating dairy cows' diet reduces enteric methane emission by over 50 percent. *J. Cleaner Prod.* 234, 132–138 (2019)
50. Wood, J., Kennedy, F.S., Wolfe, R.: Reaction of multihalogenated hydrocarbons with free and bound reduced vitamin b12. *Biochemistry* 7(5), 1707–1713 (1968)
51. Romero Perez, A., Okine, E., McGinn, S., Guan, L., Oba, M., Duval, S., et al.: Sustained reduction in methane production from long-term addition of 3-nitrooxypropanol to a beef cattle diet. *J. Anim. Sci.* 93(4), 1780–1791 (2015)
52. Duin, E.C., Wagner, T., Shima, S., Prakash, D., Cronin, B., Yáñez Ruiz, D.R., et al.: Mode of action uncovered for the specific reduction of methane emissions from ruminants by the small molecule 3-nitrooxypropanol. *Proc. Natl. Acad. Sci.* 113(22), 6172–6177 (2016)

How to cite this article: Embaby, M.G., Sarker, T.T., AbuGhazaleh, A., Ahmed, K.R.: Optical gas imaging and deep learning for quantifying enteric methane emissions from rumen fermentation *in vitro*. *IET Image Process.* 19, e13327 (2025). <https://doi.org/10.1049/ipr2.13327>